Sensors & Transducers, Vol. 227, Issue 11, November 2018, pp. 28-34

www.sensorsportal.com

Sensors & Transducers

Published by IFSA Publishing, S. L., 2018
http://www.sensorsportal.com

Surface-Potential Based Sub-Circuit Model of AlGaN/GaN HEMT Including Non-Quasi-Static Effects

Nebojsa Jankovic
Faculty of Electronic Engineering Nis, University of Nis, Aleksandra Medvedeva 14, Nis, Serbia
Tel: +381 18 529 338
E-mail: nebojsa.jankovic@elfak.ni.ac.rs

Received: 31 July 2018 /Accepted: 28 September 2018 /Published: 30 November 2018

Abstract: In this paper, the non-quasi-static surface-potential-based large signal model of AlGaN/GaN HEMT yielding continuous static and dynamic characteristics in the whole operation range is described. The model includes some important physical phenomena affecting device DC and transient operation like two-dimensional electron gas quantization, polarization charge, electron velocity saturation, high-field mobility degradation, channel length modulation and the related effect of finite time for the channel charge to build-up. The non-quasi-static HEMT model is implemented in PSPICE in the form of the equivalent sub-circuit. An excellent fit between the new HEMT model and the device numerical simulation data obtained from a TCAD software is achieved for the DC, AC and switching characteristics of normally-on GaN HEMTs with various channel lengths ranging from 1 μm to 10 μm. It is also demonstrated that, unlike the NQS model, the quasi-static (QS) modeling approach results in significant errors in predicting the fast switching transient currents of longer channel GaN HEMTs.

Keywords: Surface-potential, Sub-Circuit, AlGaN/GaN, HEMT Model.

1. Introduction

With significant progress in the improvements of quality and performance of GaN HEMTs, the exploitation of full potential of these devices requires the advanced electrical models for circuit simulations. Most GaN HEMT compact models [1-2] are based on the quasi-static (QS) assumption that ignores the finite time for the 2DEG channel charge to build-up. The QS assumption results in negligible errors in ultra-short channel devices and/or when they operate at slow rate of change of the terminal voltages that gives enough time for the channel charges to redistribute. However, at very high signal frequencies and/or in case of longer channel GaN HEMTs, the QS models result in significant errors in time-domain device simulations. A few Non-Quasi-Static (NQS) GaN HEMT models taking into account the channel charge redistribution at fast voltage transients have been proposed so far [3-5]. However, they are either empirical models fitting their equations to measured data with mathematical optimization [3] or developed only for a small-signal analysis [4-5].

In this paper, we describe the unified large/small signal NQS model of AlGaN/GaN HEMT with Schottkey gate and its implementation in SPICE. It is based on the surface-potential (SP) modelling approach also used previously for deriving the NQS models of HEMTs and MOSFETs [6-7]. The GaN HEMTs with variable channel lengths L=(1 μm÷10 μm) are analyzed in order to emphasize the importance of the NQS channel effects. Note that GaN HEMTs with longer channels (L>1μm) are often encountered in high power devices [8] or for some specific experimental and testing purposes [9-10]. The accuracy of the NQS GaN HEMT modelling is validated in this study by comparisons with t.

2. The NQS HEMT Model

Fig. 1 shows the Surface-Potential based Sub-Circuit (SPSC) model of GaN HEMT that is implemented in PSPICE circuit simulator. Unlike the similar QS SP model [12] where the gate capacitor node is simply lumped with both the external source and drain nodes, the 2DEG channel of GaN HEMT is represented in the NQS SPSC model with the N-segmental equivalent non-linear RC line as shown in Fig. 1.

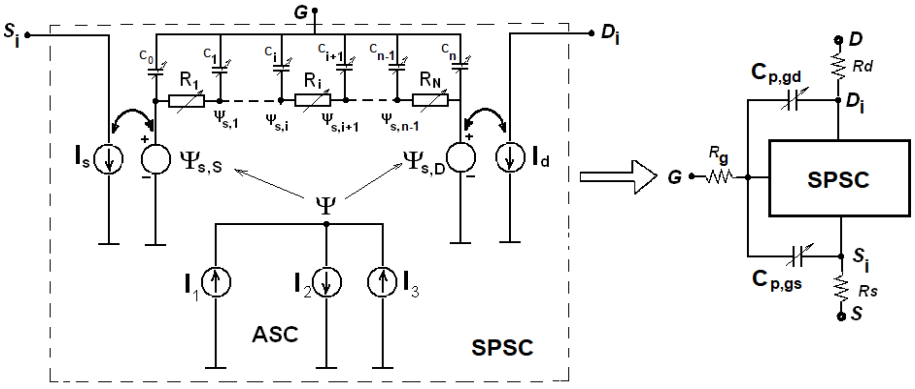


Fig. 1. The equivalent NQS SPSC model of GaN HEMT with added parasitic elements.

The core model also includes the auxiliary sub-circuit (ASC) computing the boundary surface potentials $\psi_{s,S}$ and $\psi_{s,D}$ at the source and drain ends of the channel, respectively, while the main sub-circuit (SPSC) calculates the drain and the source currents I_d and I_s, respectively, in SPICE simulations. The SPSC actually emulates the static and the dynamic operation of the intrinsic part of GaN HEMT structure. It can be embedded in the network of added extrinsic elements referring to the source/drain access regions, the gate Schottkey diode, the parasitic capacitances, inductances and resistances. In present study, only the parasitic gate-source and the gate-drain capacitances $C_{p,gs}$,$C_{p,gd}$, the gate resistance R_g and the source/drain access region ohmic resistances R_s, R_d are included in the NQS model as shown in Fig. 1. The channel segmental resistance R_i is analytically expressed as [13]:

$$R_i = \frac{w_i \cdot \left(1 - \boldsymbol{\lambda} \cdot V_{DS}^{\mathbf{m}}\right)}{W \cdot q \cdot \mu_n \cdot n_{s,i}} \tag{1}$$

where λ and m are the fitting parameters of the channel length modulation effect, $n_{s,i}$ is the channel charge density, μ_n is the electron mobility, $w_i = L/N$ is the segmental resistor length, L is the total gate length, W is the channel width and q is the electron charge. The longitudinal and vertical electric filed dependences of μ_n are modelled in (1) using the approximate physical expressions [13]. Note that the channel longitudinal electric field E_x affecting μ_n can be obtained from seeing Fig.1 as:

$$E_x = \frac{\psi_i - \psi_{i-1}}{w_i} \tag{2}$$

Finally, the channel charge density $n_{s,i}$ of the i^{th} segment was found to be quite accurately expressed with linear function [13]:

$$n_{s,i} \cong a \cdot \left(V_{gp} - \psi_i\right) + b, \tag{3}$$

where $V_{gp} = V_{gs} - V_{off}$ is the effective gate voltage, V_{off} is the channel cut-off voltage, ψ_i is the local channel potential, and a and b are the model fitting parameters.

The distributed line variable capacitors C_i are defined in the NQS model as:

$$C_i = \left(q \cdot \frac{W}{w_i} \cdot \frac{\partial n_{s,i}}{\partial V_{gs}} + \frac{C_{dep}}{N}\right), \tag{4}$$

where the first derivative term denotes the channel charge differential capacitance, while C_{dep} is the fixed gate capacitance of fully depleted AlGaN buffer layer. It can be shown from (3) and using the results presented in [12], that the derivative of $n_{s,i}$ in (4) can be quite accurately approximated by an analytical parametric function:

$$\frac{\partial n_{s,i}}{\partial V_{gs}} = a \cdot \left[1 - \frac{1}{1 + \exp\left(m \cdot V_{gp} - p \cdot V_{ds} + l\right)}\right], \tag{5}$$

where m, p and l are the new fitting parameters for modelling the variable channel capacitances C_i. Note that the parasitic capacitors $C_{p,gs}$ and $C_{p,gd}$ of the source/drain access regions can also be modelled with (4) and (5) by appropriate parameter adjustments and by taking $V_{ds}=0$ and $V_{ds}=V_{dg}$ for $C_{p,gs}$ and $C_{p,gd}$, respectively. Note that the voltage dependence of R_s and R_d as well as the drain-to-source parasitic capacitance, omitted in this study, have minor effect on the long-channel HEMT characteristics.

3. TCAD Simulations and Model Calibration

The validity of the NQS GaN HEMT model is accessed by comparisons of SPICE results with 2-D device simulations using TCAD software ATLAS from SILVACO [11]. Fig. 2 shows the schematic cross-section of an un-doped Schottkey gate $Al_{0.25}GaN_{0.75}$ HEMT structure that is simulated in this work.

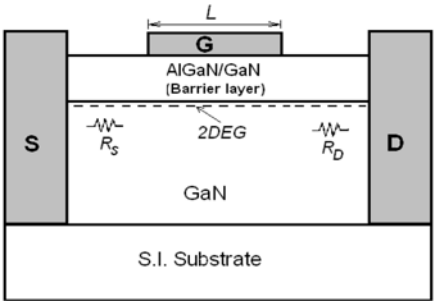


Fig. 2. A schematic cross-section of AlGaN/GaN HEMT.

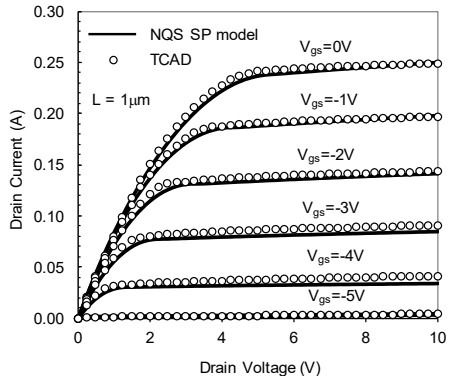
In simulations, we have adopted 400 μm, 4 μm, 32 nm and 5 eV for the device width, the length of source/drain access regions, the thickness of AlGaN barrier layer and the gate metal workfunction, respectively. The cut-off voltage of this device was found to be V_{off} = -5.5 V. Also, the Albrecht, *et al.* [14] low field electron mobility model in 2-DEG channel, the standard lateral field mobility model with velocity saturation and the ATLAS built-in polarization model for GaN devices [11] were also included in ATLAS simulations. Note that the thermal effects (device self-heating) are not included in present study.

Fig. 3 shows the comparisons between simulated and modelled the DC output characteristics of the device shown in Fig. 2 with various channel lengths L (1 μm, 6 μm and 10 μm). An excellent agreement between simulated and modelled curves is achieved by fine tuning the NQS HEMT model fitting parameters listed in [13] while keeping N=10 in all cases.

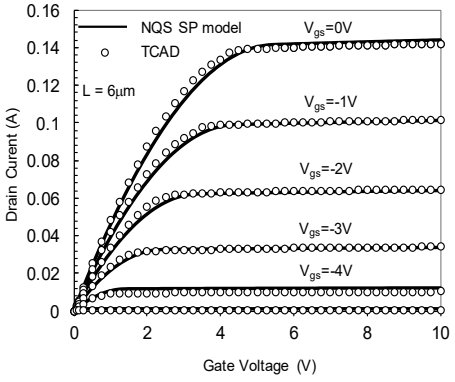
Following the DC model calibration, the parameters of voltage dependent capacitances C_i, $C_{p,gs}$ and $C_{p,gd}$ were extracted from fine tuning the modelled and simulated y-parameters obtained from ATLAS small-signal device simulations at low frequency (300 Hz) and for various V_{gs} and V_{ds}. Fig. 4 shows the good agreement between simulated and modeled the total gate input capacitance C_{GG} and the gate-drain parasitic capacitance C_{GD} versus V_{ds} and V_{gs} obtained for HEMT with L=1 μm.

4. Large Signal Modeling Results

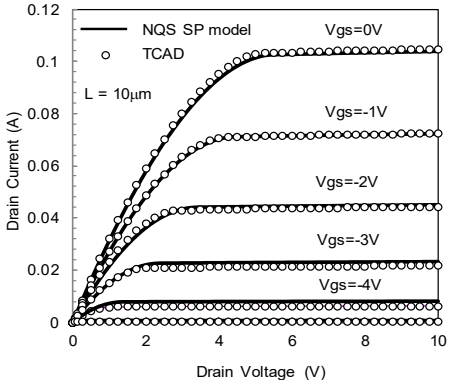
A successful calibration of the capacitance models enables the achievement of a good agreement between the simulation and modeling of the pulse transient currents in GaN HEMTs with various channel lengths (1 μm÷10 μm). The excellent agreement is obtained as shown in Fig. 5. In these simulations, the gate pulse 0 V to -5 V, the 5 V power supply and the 10 Ohms external resistor were assumed for single HEMT resistive invertor as shown in the inset of Fig. 5 (b).



(a)



(b)

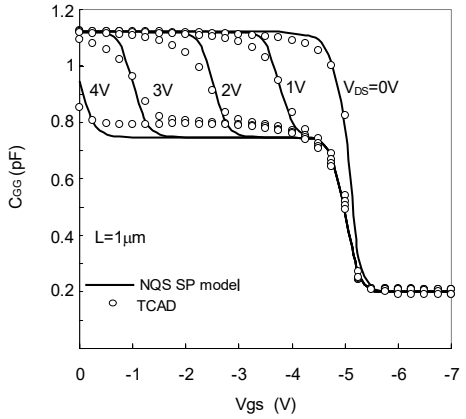


(c)

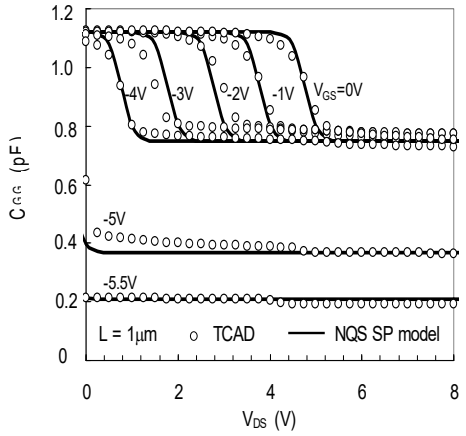
Fig. 3. Simulated and modeled the output characteristics of GaN HEMT with (a) L =1 μm, (b) L =6 μm and (c) L=10 μm.

Fig. 6 shows the NQS and QS modeling results in comparison with the TCAD mixed-mode simulations of the same invertor in case of HEMT with L=6 μm.

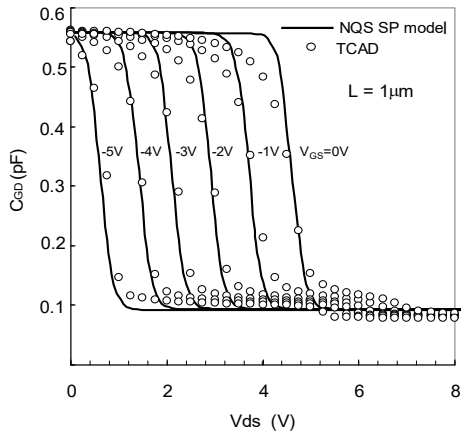
While the drain current transients are very well predicted by both models as observed in Fig. 6 (a), the QS model fails to correctly predict the source and the gate transient currents either by missing or overestimating the current spikes, respectively, as clearly shown in Fig. 6 (b) and Fig. 6 (c). The same drawback of the QS modelling approach is also found for all other simulated GaN HEMTs with L>1 μm.



(a)

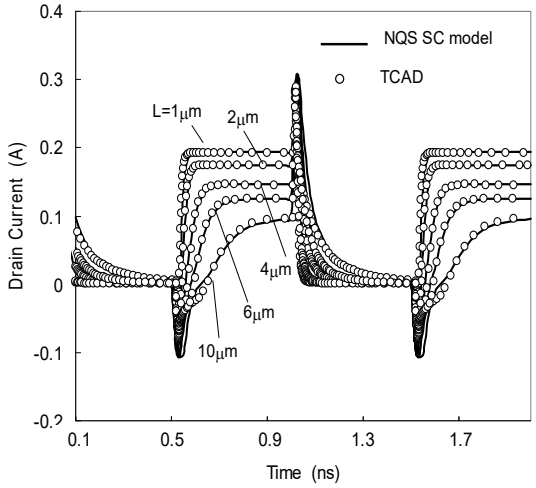


(b)

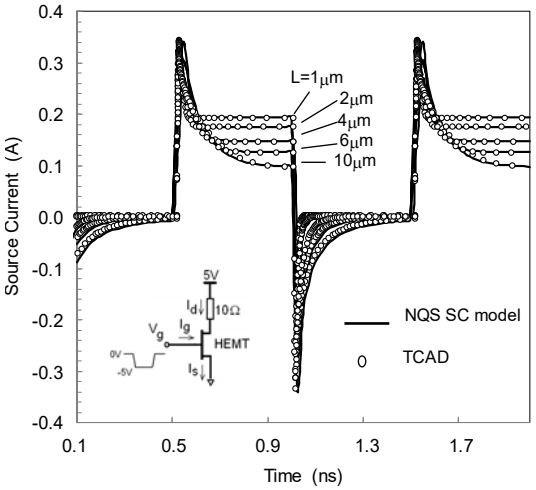


(c)

Fig. 4. Simulated and modeled the total gate input capacitance C_{GG} (a), (b); and the gate-drain capacitance C_{GD} (c) versus V_{DS} and V_{GS}.



(a)



(b)

Fig. 5. Simulated and modeled: (a) the drain and (b) the source pulse transient currents of GaN HEMTs with L=(1 μm÷10 μm). The currents were extracted from ATLAS mixed-mode and SPICE simulations of simple resistive HEMT invertor shown in the inset of (b).

5. Small-signal Modeling Results

The efficiency of the NQS model in small-signal analysis of GaN HMETs is demonstrated in Fig. 7.

It shows the comparison between the NQS modeled and TCAD simulated frequency dependences of imaginary and real parts of the input and the transfer admittances $\mathbf{y}_{11}$ and $\mathbf{y}_{12}$, respectively, of GaN HEMTs with L=1 μm, 6 μm and 10 μm at V_{gs}=0 V and V_{ds}=2 V. Because of their gate areal dependences, the absolute values of R_g and C_{dep} had to be adjusted in each case of L_g for obtaining the best fit. With increasing L_g, however, the value of gate ohmic resistance R_g decreases while the input gate capacitance C_{dep} increases, thus limiting the absolute rise of the imaginary part of $\mathbf{y}_{11}$ and $\mathbf{y}_{12}$ with frequency as shown in Fig. 7 (b) and Fig. 7 (c).

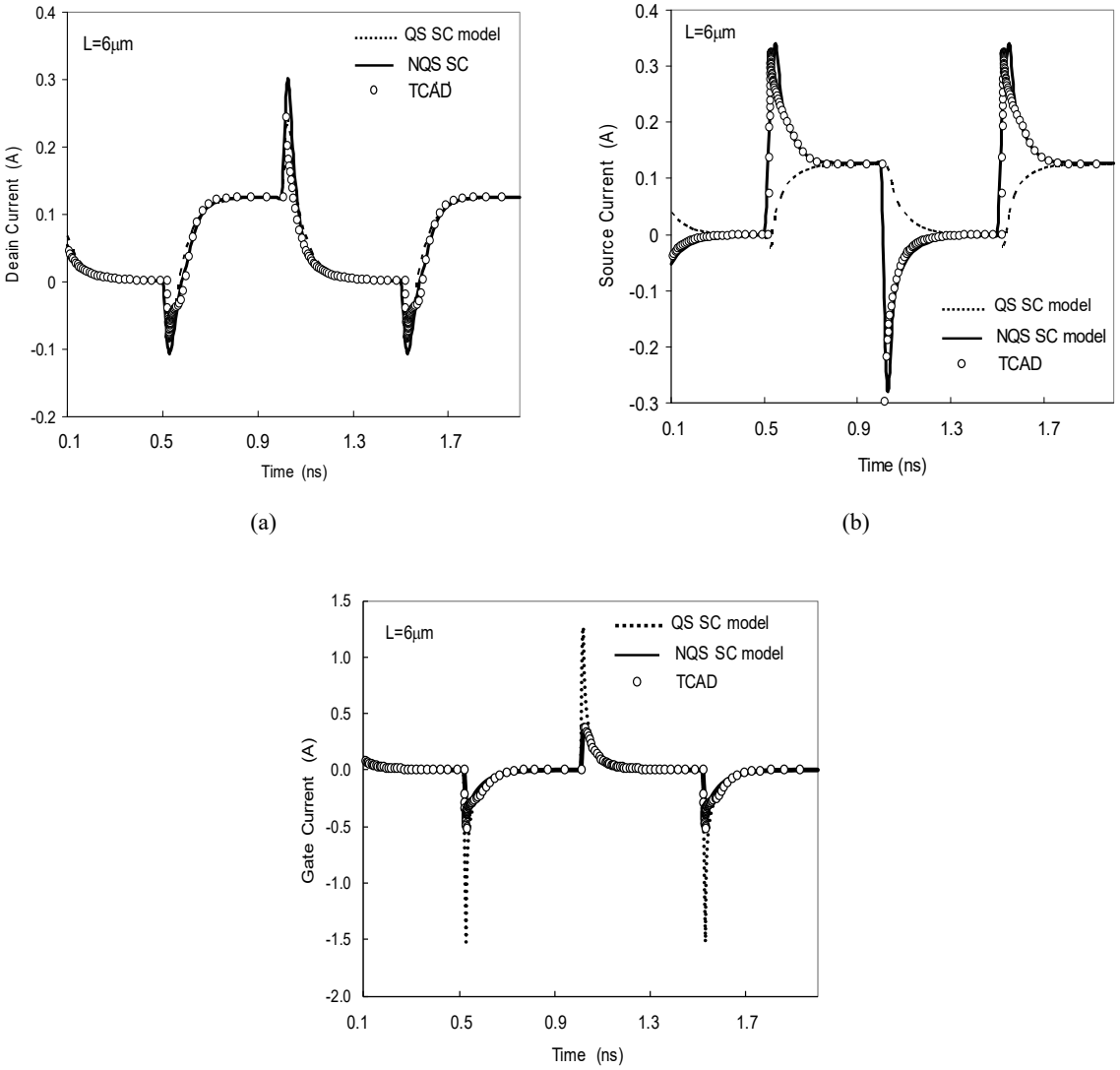


Fig. 6. Comparisons between the TCAD mixed-mode simulations and the NQS and the QS modeling of pulse transient currents (a) I_d, (b) I_s and (c) I_g of GaN HEMTwith L= 6 μm.

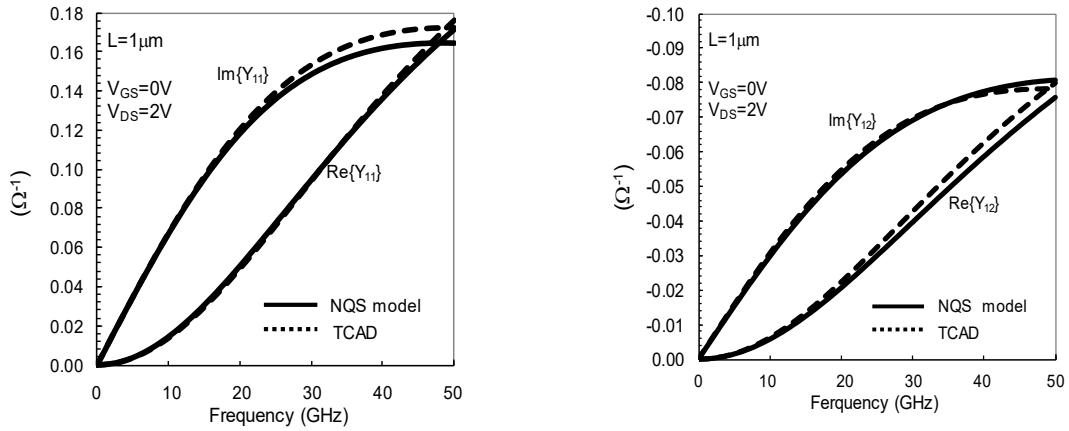


Fig. 7 (a). Simulated and modeled the imaginary and the real parts of $\mathbf{y}_{11}$ and $\mathbf{y}_{12}$ small-signal admittances versus the frequency obtained for GaN HEMT with L=1 μm at V_{gs}=0 V and V_{ds}=2 V.

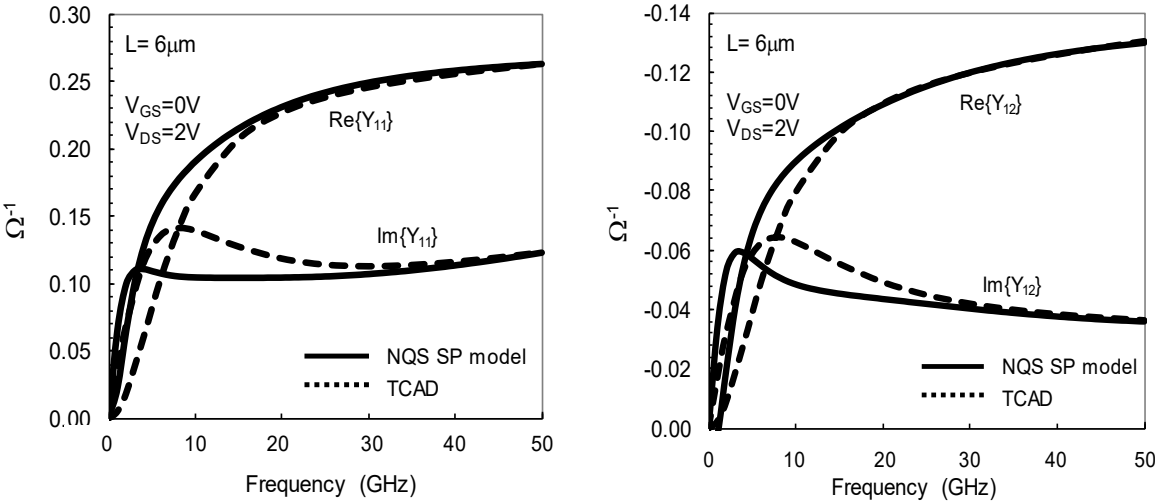


Fig. 7(b). Same as in Fig. 6(a) but for HEMT with L=6 μm.

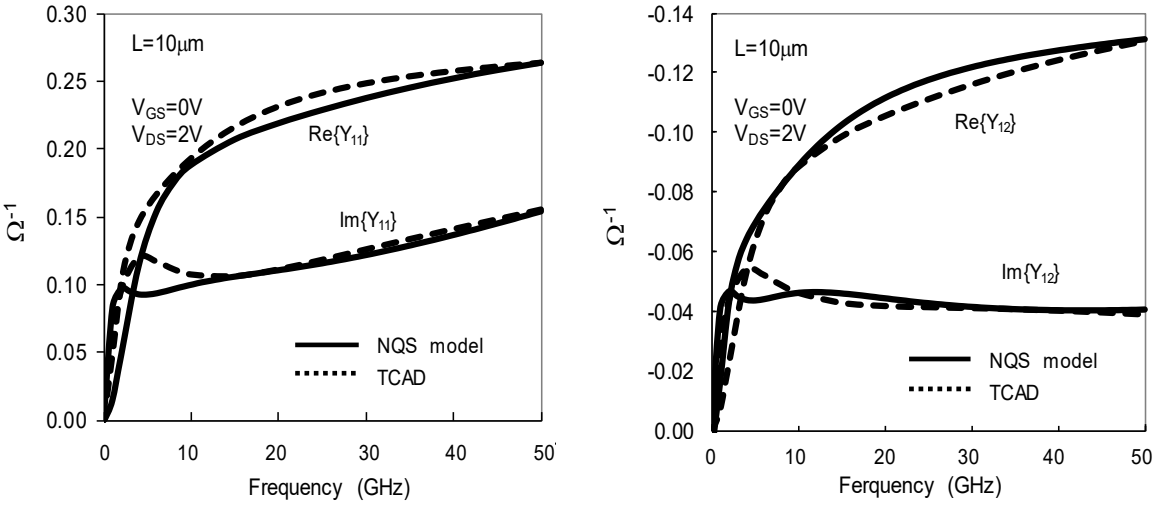


Fig. 7(c). Same as in Fig. 6(a) but for HEMT with L=10 μm.

6. Conclusions

A unified large/small signal non-quasi-static model of AlGaN/GaN HEMT with Schottkey gate is described and implemented in SPICE in the form of sub-circuit. High accuracy of the NQS model is demonstrated for both large and small signal analysis of long channel GaN HEMTs based on the comparison with two-dimensional mixed-mode numerical device simulations.

References

[1]. Chen Q., Latest advances in gallium nitride HEMT modeling, in *Proceedings of the 12th IEEE International Conference on Solid-State and Integrated Circuit Technology (ISCIST)*, 2014, pp. 1-4.

[2]. Shanthi J., Vimala P., Shanthi J., Vimala P., High Electron Mobility Transistor: A Review on Analytical Models, *International Journal for Innovative Research in Science & Technology (IJIRST)*, Vol. 3, 2016, pp. 103-114.

[3]. G. Crupi, A. Raffo, D. M. M. P. Schreurs, G. Avolio, V. Vadalà, S. Di Falco, A. Caddemi, G. Vannini, Accurate GaN HEMT Nonquasi-Static Large-Signal Model Including Dispersive Effects, *Microwave and Optical Technology Letters*, Vol. 53, Issue 3, 2011, pp. 692-697.

[4]. R. Chintakayala, I. Abdel-Motaleb, Small signal non-quasi-static model for AlGaN/GaN MODFETs, in *Proceedings of the 7th International Conference on Solid-State and Integrated Circuits Technology,* Beijing, China, Vol. 2, 2004, pp. 1163-1166.

[5]. W. E. Muhea, F. M. Yigletu, A. Lazaro, B. Iñiguez, Analytical high frequency GaN HEMT model for noise simulations, *Semiconductor Science and Technology*, Vol. 32, Issue 12, 2017, pp. 125012.

[6]. N. Jankovic, Non-Quasi-Static Large Signal Sub-Circuit Model of AlGaN/GaN HEMT, in *Proceedings*

of the 1st International Conference on Microelectronic Devices and Technologies (MicDAT'18), Barcelona, Spain, 20-22 June 2018, pp. 55-57.

[7]. T. Pesic, N. Jankovic, A Compact Non-Quasi-Static MOSFET Model based on the Equivalent Non-Linear Transmission Line, *IEEE Trans. Computer-Aided-Design Integrated Circ. Systems*, Vol. 27, Issue 10, October 2005, pp. 1550-1561.

[8]. Johnson J. W., Baca A. G., Briggs R. D., Shul R. J., Monier C., Ren F., Pearton S. J., Dabiran A. M., Wowchack A. M., Polley C. J., Chow P. P., Effect of gate length on DC performance of AlGaN/GaN HEMTs grown by MBE, *Solid-State Electronics*, Vol. 45, 2001, pp. 1979–1985.

[9]. M. Tomaska, T. Lalinsky, G. Vanko, M. Misun, Microwave Characterization and Properties of 2 μm Gate Length AlGaN/GaN HEMT Structures, in *Proceedings of the 14th Conference on Microwave Techniques*, Prague, 2008, pp. 1-4.

[10]. Cui P., Mo J., Fu C., Lv Y., Liu H., Cheng A., C. Luan, Y. Zhou, G. Dai, Lin Z., Effect of Different Gate Lengths on Polarization Coulomb Field Scattering Potential in AlGaN/GaN Heterostructure Field-Effect Transistors, *Scientific Reports*, Vol. 8, Issue 1, 2018, pp. 9036.

[11]. ATLAS User's Manual, Device Simulation Software, SILVACO International, Santa Clara, 2017.

[12]. J. Liu, Z. P. Yu, L. L. Sun, An Accurate Surface-Potential Based Large-Signal Model for HEMTs, *International Conference on Simulation of Semiconductor Processes and Devices*, 2012, pp. 4-2.

[13]. N. Jankovic, S. Faramehr, P. Igić, A Surface-Potential Based Sub-Circuit Model of I-V Characteristics, in AlGaN/GaN HEMTs, in *Proceedings of the Small System Simulation Symposium, (SSSS'18),* Niš, Serbia, 12-14 February 2018, pp. 89-95.

[14]. Albrecht J. D., Wang R. P., Ruden P. P., Farahmand M., Brennan K. F., Electron transport characteristics of GaN for high temperature device modeling, *J. Appl. Phys.,* Vol. 83, Issue 9, 1998, pp. 4777-4781.

Published by International Frequency Sensor Association (IFSA) Publishing, S. L., 2018 (http://www.sensorsportal.com).

